Journal of Power Sources 261 (2014) 264–270

Contents lists available at ScienceDirect

Journal of Power Sources

journal homepage: www.elsevier.com/locate/jpowsour

Three-dimensional aluminum foam/carbon nanotube scaffolds as long- and short-range electron pathways with improved sulfur loading for high energy density lithium–sulfur batteries

Xin-Bing Cheng [a], Hong-Jie Peng [a], Jia-Qi Huang [a,*], Lin Zhu [a,b], Shu-Hui Yang [a], Yuan Liu [c], Hua-Wei Zhang [c], Wancheng Zhu [b], Fei Wei [a], Qiang Zhang [a,*]

[a] Beijing Key Laboratory of Green Chemical Reaction Engineering and Technology, Department of Chemical Engineering, Tsinghua University, Beijing 100084, China
[b] Department of Chemical Engineering, Qufu Normal University, Shandong 273165, China
[c] School of Materials Science and Engineering, Tsinghua University, Beijing 100084, China

HIGHLIGHTS

- 3D Al foam/carbon nanotube scaffolds were applied as the current collectors.
- Short- and long-range electron pathways were efficiently constructed in a Li–S cell.
- A high discharge capacity of 6.02 mAh cm^{-2} (860 mAh g^{-1}) can be achieved on the cathode with sulfur loading of 7.0 mg cm^{-2}.

GRAPHICAL ABSTRACT

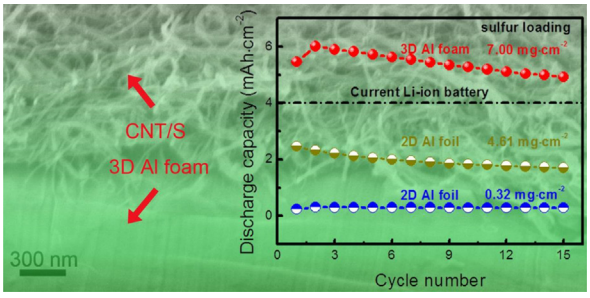

ARTICLE INFO

Article history:
Received 2 January 2014
Received in revised form
9 February 2014
Accepted 19 March 2014
Available online 27 March 2014

Keywords:
Lithium–sulfur battery
Current collector
Electron pathway
Carbon nanotube

ABSTRACT

Conductive carbon scaffolds are efficient and effective to build advanced carbon/sulfur composite cathodes for lithium–sulfur (Li–S) batteries. However, the areal sulfur loading is commonly less than 4.0 mg cm^{-2}, which limits the energy density and practical application of Li–S cells. In this contribution, three-dimensional (3D) aluminum foam/carbon nanotube (CNT) scaffolds were applied as the current collectors to build long- and short-range electron pathways and provided enough space for high sulfur loading. The sulfur loading amount on the 3D current collectors ranged from 7.0 to 12.5 mg cm^{-2}. A high initial discharge capacity of 6.02 mAh cm^{-2} (860 mAh g^{-1}) was achieved on an electrode with an improved sulfur loading of 7.0 mg cm^{-2}. Therefore, the combination of 3D long-range current collectors and short-range CNT conductive scaffold provides an efficient and effective route to make full use of sulfur with a very high sulfur loading amount in a Li–S cell.

1. Introduction

With the rapid development of the portable electronic devices and laptops, the battery performance becomes a bottleneck. Up till now, tremendous efforts from scientific and engineering communities have been devoted in improving the energy density both in weight and volume of lithium-ion (Li-ion) batteries based on

* Corresponding authors. Tel.: +86 10 62789041; fax: +86 10 62772051.
E-mail addresses: jqhuang@tsinghua.edu.cn (J.-Q. Huang), zhang-qiang@mails.tsinghua.edu.cn, zhangqiangflotu@mail.tsinghua.edu.cn (Q. Zhang).

http://dx.doi.org/10.1016/j.jpowsour.2014.03.088
0378-7753/

intercalation mechanism, which are nearly approaching their theoretical limits but still could not meet the requirements of personal electronics [1]. More importantly, the latest environmentally friendly electric vehicles (EVs) are in urgent need of advanced energy storage systems with high energy and power density, which can render EVs to be competitive to the vehicles with fossil fuel. Lithium–sulfur (Li–S) battery is one of the potential electrochemical systems with the capacity of 1675 mAh g^{-1} (based on cathode sulfur) and energy density of 2600 Wh kg^{-1} (based on Li–S redox couple), which is nearly five times more than the traditional Li-ion batteries [2–5]. Moreover, the elemental sulfur, as a common industrial by-product, also exhibits advantages of low cost, environmental friendliness, and natural abundance [6].

Apart from its advantages in theoretical calculation, Li–S battery suffers from several practical obstacles. Firstly, the insulative nature of sulfur (an ultra-low electron conductivity of 5×10^{-30} S cm^{-1} at room temperature) results in a poor electrochemical kinetics and low utilization, which has been well addressed by the addition of the conductive scaffolds (*e.g.* ordered mesoporous carbon [7–10], carbon nanotubes (CNTs) [11–14], graphene [15,16], CNT/graphene hybrids [17], carbon hollow spheres [18], carbide-derived carbon [19], hierarchically porous carbon [20,21], polyacrylonitrile [22], etc.). However, the large amount addition of conductive materials hinders the full demonstration of the high energy density of Li–S cells. Secondly, during the discharge processes, higher-order polysulfides generate, then dissolve into the bulk electrolyte, and shuttle between anode and cathode, which severely degrades the discharge capacity and long-term stability of Li–S batteries. Several strategies (such as trapping the sulfur in the cathode [9,10,14,23–26], an ion selective membrane [27], as well as lithium nitrate ($LiNO_3$) addition [28]) have been proposed to shied the polysulfide shuttle. Finally, the sulfur loading (the amount of sulfur in the whole electrode) significantly affects the gross capacity of the electrode and the energy density of the total cell, which, however, is usually ignored in previous reports. The areal loading density and the capacity of the reported electrode are, respectively, much lower than 4.0 mg cm^{-2} and 4.0 mAh cm^{-2}, which is desired for the industrial society towards practical Li–S cells with compatible energy density to current Li-ion batteries [29]. Conventional two-dimensional (2D) aluminum (Al) foils as current collectors can only support sparsely limited active weight. Thus, it is highly expected to explore effective strategy for efficiently loading sulfur phase in the cathode with high capacity, good utilization, robust framework, as well as excellent cycling performance.

The one-dimensional (1D) CNTs exhibit ultrahigh conductivity ($>10^3$ S m^{-1}). The multi-walled CNTs produced by fluidized bed chemical vapor deposition possess a very low cost (less than \$100 kg^{-1}) and robust mechanical properties that can withstand volume changes during long-cycle charge–discharge process [30,31]. This is especially beneficial for the construction of a robust conducting network as short-range electron pathways. Therefore, CNTs have been strongly recommended as conductive fillers with quite high sulfur loading capability in a Li–S cell [32]. The use of nanocarbon as short-range conductive networks is quite efficient and effective for the line-to-point contact, and the current applied on each CNT is mostly collected by the plate Al foil through point/line-to-plate contact in the above mentioned researches. In some cases, the short-range CNT conductors are detached from the Al foil due to the unexpected random expansion at the CNT/sulfur–Al foil interface. With the increasing of sulfur loading, the pathways of electron from the Al foil to the sulfur become longer, consequently, the diffusion of ions through the thick electrode is restrained, which hinder the full use of sulfur for Li ion storage. Thus, designing the whole configuration of current collectors for the efficient multi-range electron/ion transfer is highly considered.

In this contribution, a 3D Al foam instead of routine 2D Al foil was employed as the long-range conductive matrix. The combination of 3D Al foam with CNT frameworks not only exhibits long-/short-range scaffolds as electron pathways through hierarchical point-line-plate contact, but also offers vast void space to accommodate huge amount of active materials and interconnected channels with short diffusion pathways and low resistance. A high sulfur loading of 7.0 mg cm^{-2} (based on the surface area of the electrode) was available with a discharge capacity of 6.02 mAh cm^{-2} (860 mAh g^{-1}) at a current density of 1.17 mA cm^{-2} (167 mA g^{-1}). This was much higher than the Li–S cell with routine Al foil current collectors.

2. Experimental

2.1. Fabrication of composite cathode

The CNTs were mass-produced on Fe based catalysts in a fluidized bed reactor [33]. The as-grown carbon products were purified by sodium hydroxide (12.0 mol L^{-1}) aqueous solution at 160 °C for 4.0 h and hydrochloric acid (5.0 mol L^{-1}) aqueous solution at 70 °C for 4.0 h, subsequently. The high purity CNT bundles were available after filtering, washing, and freeze–drying. Then the CNTs were mixed with sulfur powder in the anticipated mass ratio of 1:1 and ball-milled for 3.0 h to form CNT/sulfur composites.

2.2. Structure characterizations

The structure of the cathode was identified by an X-ray diffractor (XRD, D8-Advance, Bruker, Germany). A JSM 7401F scanning electron microscopy (SEM, JEOL Ltd., Tokyo, Japan) and a transmission electron microscopy (TEM, JEOL Ltd., Tokyo, Japan) were employed to detect the morphology of raw materials and composite electrodes. The sulfur content of CNT/sulfur composite was determined as 50% (Fig. S1) by thermal gravimetric analysis (TGA) using TGA/DC1 STAR^e system in N_2 atmosphere at a temperature ramp rate of 10 °C min^{-1}. The N_2 adsorption–desorption isotherms were collected by using a N_2 adsorption analyzer (Autosorb-iQ_2-MP-C system) at 77 K. The sample was degassed at a low temperature of 50 °C until a manifold pressure of 2.0 mmHg was reached before N_2 sorption isotherm measurements to avoid the sulfur sublimation. The surface area was determined by the Brunauer–Emmett–Teller (BET) method, and the pore size distribution plot was calculated by the nonlocal density functional theory.

2.3. Li storage performance of composite cathode

The composite CNT/sulfur cathode was fabricated with poly(-vinylidene fluoride) (PVDF) binder in *N*-methyl-2-pyrrolidone (NMP) with a mass ratio of CNT:sulfur : PVDF = 42.5:42.5:15. A homogeneously mixed slurry was prepared by magnetic stirred for 24.0 h. The slurry was then coated onto a Al foam with a controllable sulfur loading amount ranging from 7.0 to 12.5 mg cm^{-2}, which was punched into 13.0 mm disks. The Al foam fabricated by an artificial punched method was with a bulk density of 0.34 g cm^{-3}, a porosity of 0.88, a bulk thickness of *ca.* 150 μm, and a surface area of 0.04 m^2 g^{-1}. The obtained electrode was dried in a vacuum drying oven at 60 °C for 12.0 h. The electrodes were assembled in a two-electrode cell configuration using standard 2025 coin-type cells. Li metal foils with 1.0 mm thick was selected as counter electrodes. The mixed solution of DOL and DME ($v/v = 1/1$) dissolving 1.0 mol L^{-1} lithium bis(trifluoromethanesulfonyl) imide (LiTFSI) was employed as the electrolyte, and the Celgard 2400 polypropylene membranes as the separator. The assembling of cells was conducted in an Ar-filled glove box with oxygen and

water content below 1 ppm. The coin cells were monitored in galvanostatic mode within a voltage range of 1.0–3.0 V using a Neware multichannel battery cycler. The cyclic voltammetry (CV) and electrochemical impedance spectroscopy (EIS) measurements were performed on Solartron 1470E electrochemical workstation at a scan rate of 0.1 mV s^{-1} and frequency range of 10^{-2}–10^{5} Hz, respectively.

3. Results and discussion

The CNTs were employed as short-range conductive pathways to obtain composite cathode. The CNT/sulfur composites fabricated by room-temperature ball-milling without heating at 155 °C were shown in Fig. 1. There were large volume of mesopores among the tube bundles that provided enough space for sulfur accommodation (shown in Fig. 1a and Fig. S2). The CNT@sulfur coaxial nanocables were seldom observed, attributing from the lack of co-heating procedure, which was widely applied in many reports [13–18,25,27,34]. The sulfur was attached with CNTs and occupied the void space between the CNT bundles (Fig. 1b). This guaranteed the unblocked conductive network with well electrical contacts in the short range. The high-magnification TEM image of CNT/sulfur composites in Fig. 1b demonstrated that sulfur in the composites was well crystalline, consisting with the XRD patterns (Fig. 1c).

To construct an efficient long-range conductive network, a 3D Al foam was employed. Fig. 2a elucidated the bird view of 3D Al foam current collector, which exhibited two kinds of holes. One is the through-hole and the other is half-through-hole that can be confirmed in the partial enlarged view of Fig. 2b. The through-holes separated the Al foam into 2D square units (the green square (in the web version) in Fig. 2a) with a lattice of 450 μm. The primitive cell (the purple square in Fig. 2a) of the 3D Al foam was with a lattice of 318 μm. The combined structure consisted of opposite protuberances on a foil. The protuberances were with a diameter of 75 μm and the 3D Al foam was with a thickness of *ca* 150 μm for the 3D Al foam. Such Al foam provided more contact interfaces to create CNT/sulfur–Al junction and larger free spaces to accommodate the composite cathodes than routine flat Al foil. The current collector with the loading of 6.4 mg cm^{-2} of sulfur was shown as Fig. 2c and d. The thickness of the composites was 51 μm with 35 and 16 μm on and underneath the current collector, respectively. That gained an outstanding increase in the thickness of the composites relative to the 2D Al foil with a thickness of 10–20 μm. The high magnification SEM image elucidated the interface between CNT/sulfur composites and the 3D Al foam (Fig. 2e). The sulfur was attached to CNTs tightly while the interface between CNT/sulfur composites and the Al foam was built effectively, resulting in interconnected electron pathway from short-range to long-range.

By coating the CNT/sulfur composites to the 3D Al foam current collectors, cathodes with high sulfur loading of 7.0–12.5 mg cm^{-2} were available and assembled into coin cells to test the electrochemical performance of Li–S batteries. Fig. 3a and b showed cycling performance at a current density of 0.1C (1C = 1675 mA g^{-1}, corresponding to an areal current density of 1.17 mA cm^{-2}) on CNT/sulfur cathode with a sulfur loading of 7.0 mg cm^{-2}. A high initial discharge capacity of 6.02 mAh cm^{-2} (860 mAh g^{-1}) was achieved. In contrast, the cathodes with the 2D Al foils were only with sulfur loadings of 0.32 and 4.61 mg cm^{-2} and discharge capacities of 0.31 and 2.46 mAh cm^{-2} (964 and 534 mAh g^{-1}), respectively. The hierarchical-range conductive network built synergistically by the 3D Al foam and CNTs led to higher utilization rate of sulfur and higher sulfur loading amount

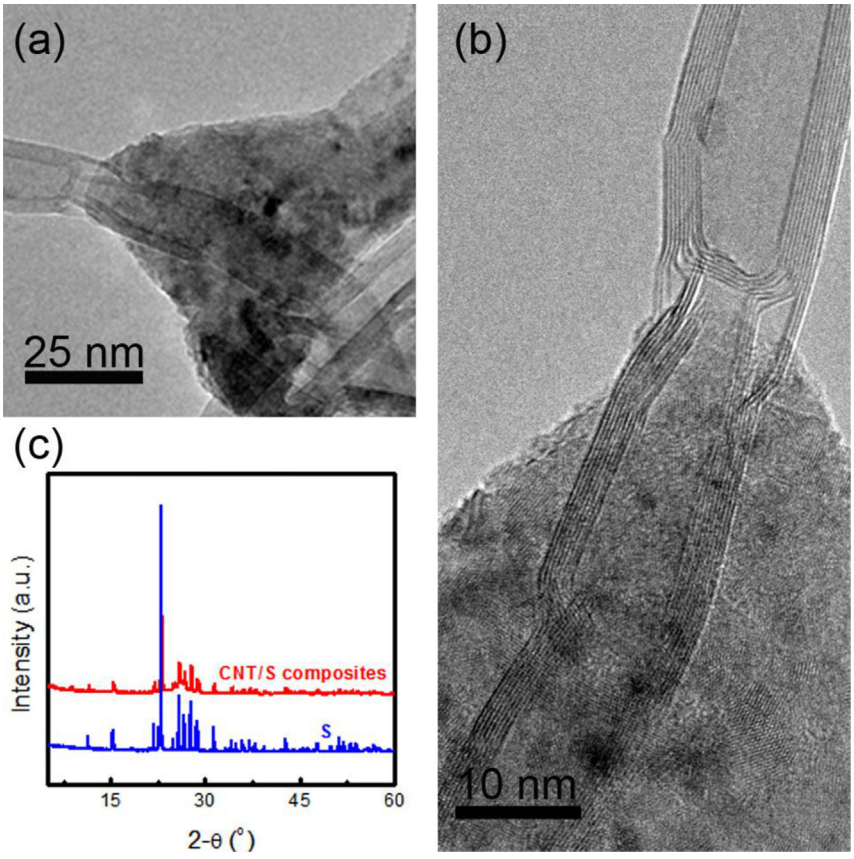

Fig. 1. (a) The low magnification TEM image of CNT/sulfur composites; (b) the joint part of CNTs and sulfur; (c) the XRD patterns of the CNT/sulfur composites and sulfur.

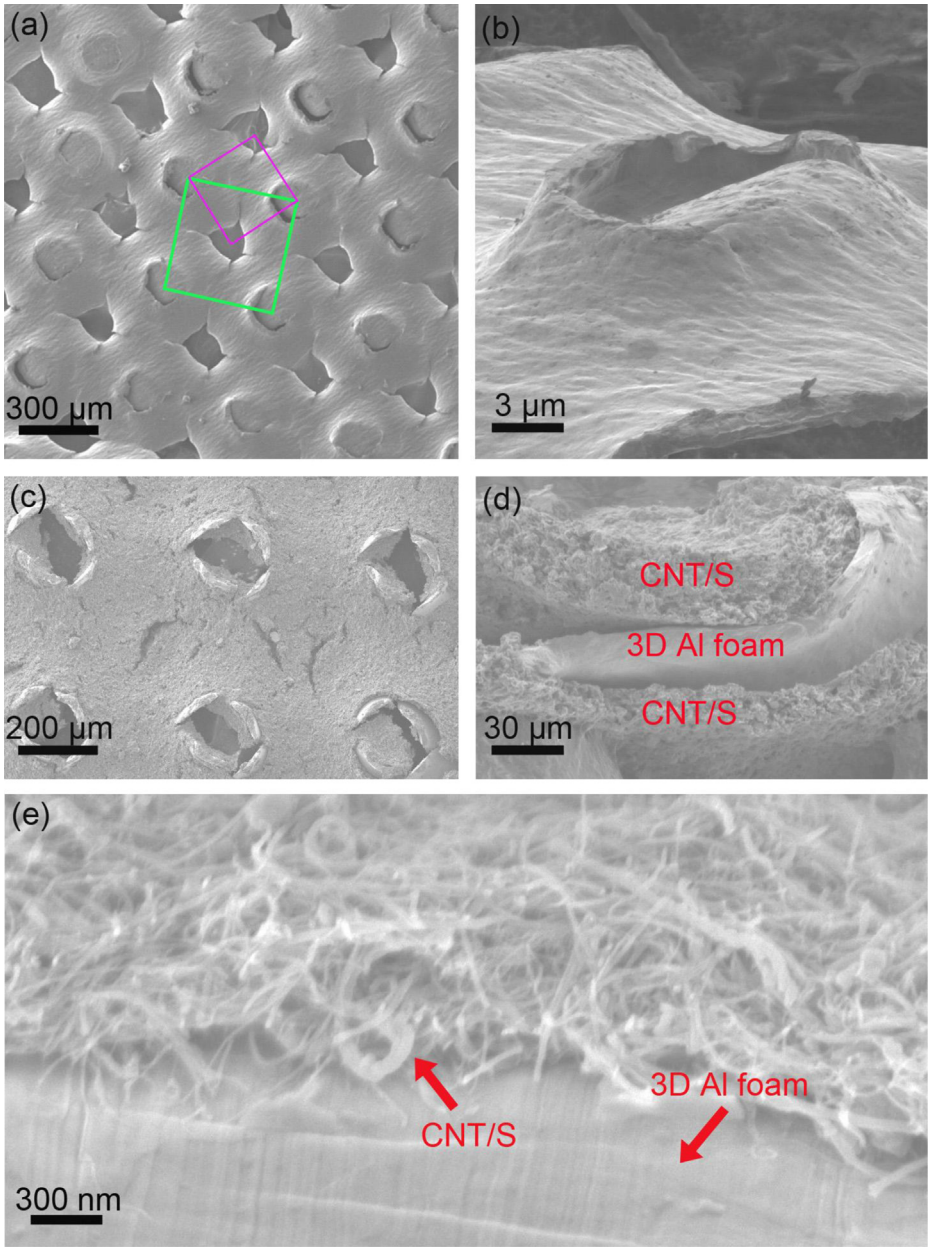

Fig. 2. The morphology of 3D Al foam current collector and related electrodes: (a) the bird and (b) side view of the Al foam current collector; (c) the bird and (d) side view of the Al foam current collector with the CNT/sulfur composite cathode; (e) the high magnification SEM image of the CNT/sulfur composites with the 3D Al foam, showing the multi-range charge-transfer interfaces.

than those on routine Al foil. The high loading of sulfur in a cell induced the increase of amount of the dissolved polysulfides, which can shuttle between the cathode and anode and led to a low Coulombic efficiency of 80%. The charge–discharge profiles of 3D Al foam/CNT/sulfur cathode (Fig. 3c) possessed a typical two-plateaus feature of Li–S battery with the high platform of 2.3 V and low platform of 2.05 V, which exhibited similar polarization compared with the cell consisting of very low loading (0.32 mg cm^{-2}) on 2D Al foil. However, much severer polarization occurred when only promoting the areal loading without employing 3D Al foam architecture. The distinct difference in electrochemical kinetics indicated that the 3D interconnected Al foam served as excellent long-range conductive scaffolds, significantly improving the charge transfer behavior across the Al–carbon–sulfur interfaces. As a result, a boost of both sulfur loading and utilization was performed by incorporating the Al foam with short-range conducting CNT scaffold.

The EIS results of the cells with the 2D Al foil and 3D Al foam were shown in Fig. 3d. A computer analysis of electrochemical impedance data [35] to minimize the sum of squares of the radial difference between observed and calculated impedance data presented in either the complex impedance or admittance plane was conducted (Table 1). The impedance (resistance) due to electrolyte and cell components, solid electrolyte interface (SEI) film, and charge transfer of the 3D current collector cathode were 4.85, 10.72, 20.61 Ω, respectively. These were a little larger than the 2D current collector cathode. The high sulfur loading in cathode with 3D current collector resulted in vast dissolution of polysulfides into the electrolyte and the irreversible deposition of Li_2S and/or Li_2S_2 on cathode, anode, and any other dead spaces in the cell, leading to the rise of related

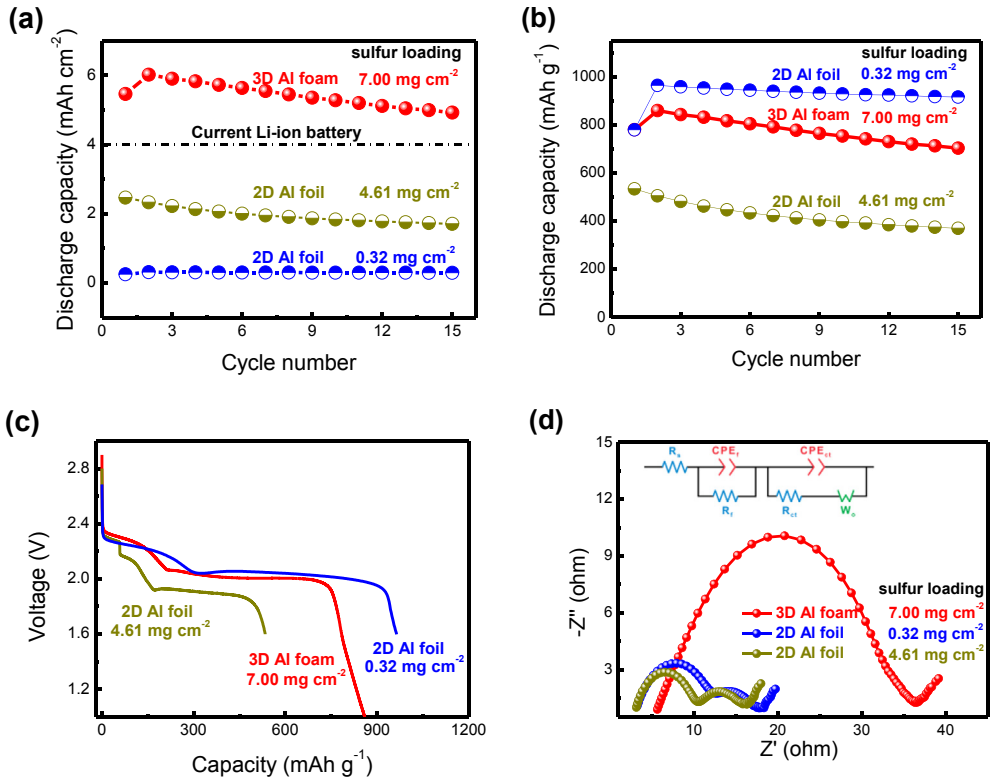

Fig. 3. The discharge capacity based on (a) the area of electrode and (b) the weight of sulfur of Li–S battery at a current density of 0.1C with the sulfur content of 7.0 mg cm^{-2} and (c) the corresponding galvanostatic charge–discharge curves; (d) the Nyquist plots and corresponding equivalent circuits for 2D Al foil and 3D Al foam.

resistances. However, the resistance of diffusion of lithium ions into the bulk cathode was less than the 2D Al foil, which was likely on account of interconnected rapid ion channels in the cathode.

The CNTs have been widely explored as scaffolds for Li–S cell. Liu and co-workers applied the CNT/sulfur composite film as a flexible cathode to obtain the total material loading density of ~5 mg cm^{-2}, corresponding to the sulfur loading of 3.25 mg cm^{-2} [36]. Abruña et al. obtained a high sulfur loading of 6.0 mg cm^{-2} and a high first discharge capacity of 800 mAh g^{-1}, corresponding to a capacity of 4.8 mAh cm^{-2} [37]. Hagen et al. carried out extremely high sulfur loadings of 3.0–15.7 mg cm^{-2} by applying a binder-free thick film electrode based on CNTs, which exhibited a high capacity of *ca.* 900 and 750 mAh g^{-1} at a current density of 0.64 mA cm^{-2}, respectively [13]. Wang et al. incorporated with CNTs with mesoporous carbon for composite microspheres that demonstrated superb battery performance with a reversible capacity over 700 mAh g^{-1} after 200 cycles at a high current density of 2.8 mA cm^{-2} [38]. With the addition of polyethylene glycol barrier on the electrode, there is a 22% increase on the discharge capacity of aligned CNT/sulfur cathode with a loading of 2.5 mg cm^{-2} [39]. Herein, an initial discharge capacity of 6.02 mAh cm^{-2} (860 mAh g^{-1}) was available on 3D Al foam/CNT/sulfur cathode with a sulfur loading of 7.0 mg cm^{-2}. In such electrode configuration, the 3D Al foam acted as long range electron pathways and the CNTs with the super conductivity acted as short range electron pathways together to build electron transport highway, which guaranteed the efficient electron transfer between the sulfur and external circuit. As shown in Table 2, an electrical conductivity of 0.62 S cm^{-1} for the 3D current collector cathode with sulfur loading of 7.0 mg cm^{-2} was obtained, which was higher than 0.53 S cm^{-1} of routine 2D Al foil with a sulfur loading 4.61 mg cm^{-2}. Therefore, the electrical conductivity of 3D current collector cathode was much improved than the sulfur (5×10^{-30} S cm^{-1}) and confirmed the unblocked conductive skeleton. Similarly the uses of other 3D conductive framework, *e.g.* 3D Ni foam [40,41], stainless-steel [42], carbon fiber woven [43–45], nano-cellular carbon [46], as well as CNT/graphene based current-collectors [47,48], are also expected to bring intimate contact between the insulating sulfur and the embedded conductive matrix. That allowed high active material loading, and facilitated efficient retention of soluble polysulfides within the 3D cathode architecture. Very recently, the mesoporous nitrogen-doped carbon–sulfur cathodes offered a high areal capacity (*ca.* 3.3 mAh cm^{-2}) at a current density of 0.7 mA cm^{-2} with a high sulfur loading (4.2 mg cm^{-2}), a sulfur content (70 wt%) on Al foil, and 10 wt% Super P conductive fillers [29]. It is highly expected that the utilization of sulfur is improved if the long-range Al current collector is employed.

Table 1
Components of the equivalent circuit fitted for the impedance spectra.

Sample	Sulfur loading (mg cm^{-2})	R_s[a] (Ω)	CPE$_f$[b] (F)	R_f[a] (Ω)	CPE$_{ct}$[b] (μF)	R_{ct}[a] (Ω)	W_o[c] (Ω s$^{0.5}$)
2D Al foil	0.32	1.64	4.30×10^{-6}	4.09	5.3	13.42	0.59
2D Al foil	4.61	2.21	3.01×10^{-6}	4.30	12	11.83	0.60
3D Al foam	7.00	4.85	1.64×10^{-5}	10.72	0.48	20.61	0.31

[a] R_s, R_f, and R_{ct} are impedance (resistance) due to electrolyte and cell components, solid electrolyte interface (SEI) film, and charge transfer, respectively.
[b] CPE is the respective constant phase element to account for the depressed semicircle in the experimental spectra.
[c] W_o is the finite length Warburg (short circuit terminus) element related to the diffusion of lithium ions into the bulk cathode.

Table 2
Summary of CNT/S cathode onto the routine 2D Al foil and the 3D Al foam.

	2D Al foil – low loading	2D Al foil – high loading	3D Al foam
Sulfur loading (mg cm^{-2})	0.32	4.61	7.00
PVDF (mg cm^{-2})	0.11	1.03	2.47
CNT (mg cm^{-2})	0.26	4.61	7.01
Current collector (mg cm^{-2})	4.24	4.24	3.97
Electrical conductivity (S cm^{-1})	1.27	0.53	0.62
Initial capacity (mAh g^{-1}_{sulfur})	964	534	860
Initial capacity (mAh cm^{-2})	0.31	2.46	6.02

To seek for the maximum permitted sulfur loading in the coin cell, a loading of 12.5 mg cm^{-2} was obtained with an initial discharge capacity of 3.12 mAh cm^{-2} and a capacity retention ratio of 81% in the 70th cycle at a relatively high current density of 2.09 mA cm^{-2} (Fig. 4a). The charge–discharge curves in Fig. 4b lost the two-platform feature. The low platform became sloping with a low voltage of 1.8 V. This can be ascribed to the close packing among CNT/sulfur agglomerates and the longer diffusion distance, which provides limited channels for both electron transfer and ion diffusion. Furthermore, such degradation of electrode kinetics in a Li–S cell with extremely high sulfur loading was also evaluated by the CV measurement (Fig. 4c). The peaks at 1.98 and 2.31 V in the cathodic scan were identified as the reactions of sulfur to higher-order polysulfides and higher-order polysulfides to lithium sulfides (Li_2S) and/or lithium disulfides (Li_2S_2), respectively [17,49]. Similarly, the weaken intensity and lower voltage of the redox peaks corresponding to the liquid-to-solid transformation of soluble polysulfides to insoluble Li_2S/Li_2S_2 further indicated the limited charge transfer property. Thus, such an extremely high loading of sulfur hindered the efficiency of the hierarchical 3D Al foam/CNT conductive scaffold but still gained much improved energy density in the cell scale when compared to the previously reported low sulfur loading cathode.

The rate performance of a Li–S cell based on 3D Al foam was demonstrated, delivering capacities of 642 (2.44), 634 (2.41), 507 (1.90), 347 mAh g^{-1} (1.32 mAh cm^{-2}) at a current of 0.1, 0.2, 0.5, and 1.0C, respectively. The Coulombic efficiency was low around 80–95%, which was attributed from the inevitable shuttle of polysulfides. It is expected that the Coulombic efficiency can be improved to around 100% if $LiNO_3$ [4,28,38,49] and/or ion selective membrane [27] are introduced into the cell system to restrain the shuttle of polysulfides. The rational design and construct long- and short-range electron pathways, together with the reported strategies to control the shuttle of polysulfides, are very effective to obtain a Li–S cell for practical applications.

4. Conclusions

A 3D Al foil and CNTs were employed as long- and short-range current collector for CNT/sulfur cathode in a Li–S cell. When the sulfur loading was 7.0 mg cm^{-2}, the cell demonstrated a high initial discharge capacity of 6.02 mAh cm^{-2} (860 mAh g^{-1}). In contrast, the cell with Al foil as current collector rendered a lower loading of 4.61 mg cm^{-2} with a lower initial discharge capacity of 2.46 mAh cm^{-2} (534 mAh g^{-1}). This is attributed from the fact that

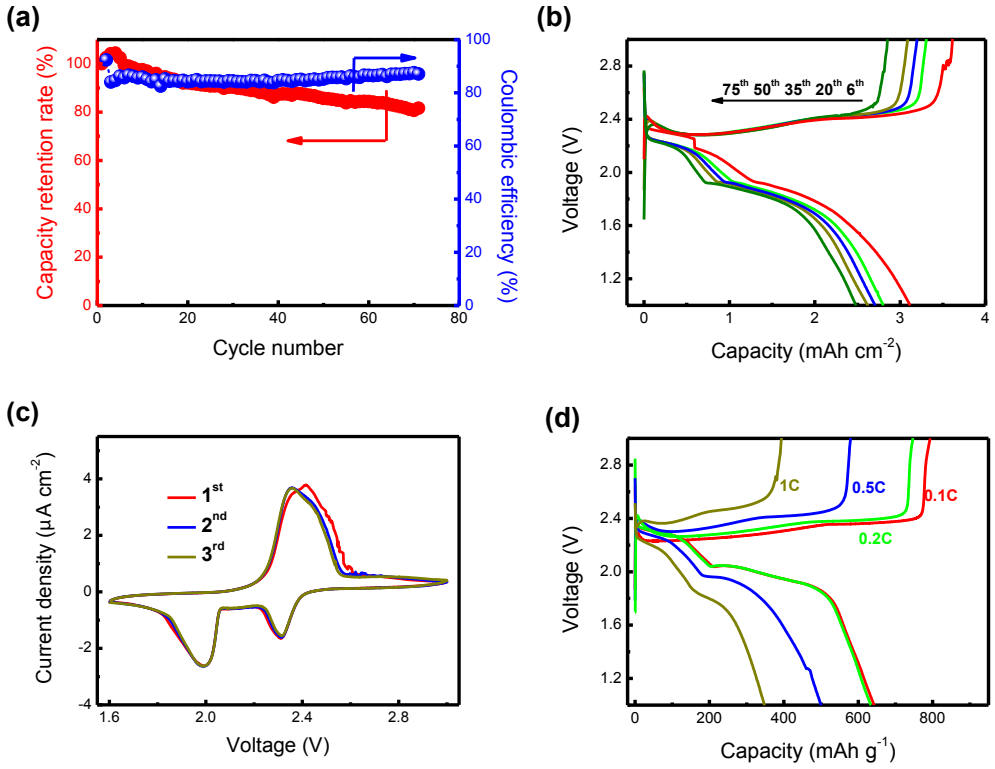

Fig. 4. (a) The long cycle performance of Li–S battery at a current density of 0.1C with an extremely high sulfur loading of 12.5 mg cm^{-2} and (b) the corresponding galvanostatic charge–discharge curves; (c) the CV curves at a scan rate of 0.1 mV s^{-1} of the cell with 3D current collector and (d) the charge–discharge curves at various current rates.

the 3D Al foil/CNT current collectors not only provides long-/short-range scaffolds as electron pathways through point-line-plate contact, but also offers vast volume to accommodate the active materials with short lithium-ion diffusion pathway and low resistance. Such strategy to hybridize macroscopic 3D current collectors and nanocarbon (CNTs, graphene) into a hierarchical 3D network is highly efficiency to build high loading electrodes with excellent Li storage performance and good economy. It also holds the potential to be applied in other electrochemical energy storage system (*e.g.* Li-ion batteries, supercapacitors, redox flow batteries, as well as Li-air batteries) towards high energy density.

Acknowledgment

This work was supported by the China Postdoctoral Science Foundation (2012M520293, 2013T60125), and National Natural Science Foundation of China (21306103), and Research Fund for the Doctoral Program of Higher Education of China (20120002120047).

Appendix A. Supplementary data

Supplementary data related to this article can be found at http://dx.doi.org/10.1016/j.jpowsour.2014.03.088.

References

[1] N.S. Choi, Z.H. Chen, S.A. Freunberger, X.L. Ji, Y.K. Sun, K. Amine, G. Yushin, L.F. Nazar, J. Cho, P.G. Bruce, Angew. Chem. Int. Ed. 51 (2012) 9994–10024.
[2] P.G. Bruce, S.A. Freunberger, L.J. Hardwick, J.M. Tarascon, Nat. Mater. 11 (2012) 19–29.
[3] M.K. Song, E.J. Cairns, Y.G. Zhang, Nanoscale 5 (2013) 2186–2204.
[4] D.W. Wang, Q.C. Zeng, G.M. Zhou, L.C. Yin, F. Li, H.M. Cheng, I.R. Gentle, G.Q.M. Lu, J. Mater. Chem. A 1 (2013) 9382–9394.
[5] S.S. Zhang, J. Power Sources 231 (2013) 153–162.
[6] A. Manthiram, Y.Z. Fu, Y.S. Su, Acc. Chem. Res. 46 (2013) 1125–1134.
[7] F.G. Sun, J.T. Wang, H.C. Chen, W.C. Li, W.M. Qiao, D.H. Long, L.C. Ling, ACS Appl. Mater. Interfaces 5 (2013) 5630–5638.
[8] M. Oschatz, S. Thieme, L. Borchardt, M.R. Lohe, T. Biemelt, J. Bruckner, H. Althues, S. Kaskel, Chem. Commun. 49 (2013) 5832–5834.
[9] X.L. Ji, S. Evers, R. Black, L.F. Nazar, Nat. Commun. 2 (2011) 325.
[10] X. Ji, K.T. Lee, L.F. Nazar, Nat. Mater. 8 (2009) 500–506.
[11] G.M. Zhou, D.W. Wang, F. Li, P.X. Hou, L.C. Yin, C. Liu, G.Q. Lu, I.R. Gentle, H.M. Cheng, Energy Environ. Sci. 5 (2012) 8901–8906.
[12] M. Hagen, S. Dorfler, H. Althues, J. Tubke, M.J. Hoffmann, S. Kaskel, K. Pinkwart, J. Power Sources 213 (2012) 239–248.
[13] M. Hagen, S. Dorfler, P. Fanz, T. Berger, R. Speck, J. Tubke, H. Althues, M.J. Hoffmann, C. Scherr, S. Kaskel, J. Power Sources 224 (2013) 260–268.
[14] S.M. Zhang, Q. Zhang, J.Q. Huang, X.F. Liu, W.C. Zhu, M.Q. Zhao, W.Z. Qian, F. Wei, Part. Part. Syst. Char. 30 (2013) 158–165.
[15] G. Zhou, L.C. Yin, D.-W. Wang, L. Li, S. Pei, I.R. Gentle, F. Li, H.M. Cheng, ACS Nano 7 (2013) 5367–5375.
[16] J.Q. Huang, X.F. Liu, Q. Zhang, C.M. Chen, M.Q. Zhao, S.M. Zhang, W.C. Zhu, W.Z. Qian, F. Wei, Nano Energy 2 (2013) 314–321.
[17] M.Q. Zhao, X.F. Liu, Q. Zhang, G.L. Tian, J.Q. Huang, W.C. Zhu, F. Wei, ACS Nano 6 (2012) 10759–10769.
[18] N. Brun, K. Sakaushi, L.H. Yu, L. Giebeler, J. Eckert, M.M. Titirici, Phys. Chem. Chem. Phys. 15 (2013) 6080–6087.
[19] J.T. Lee, Y. Zhao, S. Thieme, H. Kim, M. Oschatz, L. Borchardt, A. Magasinski, W.-I. Cho, S. Kaskel, G. Yushin, Adv. Mater. 25 (2013) 4573–4579.
[20] L. Yu, N. Brun, K. Sakaushi, J. Eckert, M.M. Titirici, Carbon 61 (2013) 245–253.
[21] S.R. Zhao, C.M. Li, W.K. Wang, H. Zhang, M.Y. Gao, X. Xiong, A.B. Wang, K.G. Yuan, Y.Q. Huang, F. Wang, J. Mater. Chem. A 1 (2013) 3334–3339.
[22] L.C. Yin, J.L. Wang, F.J. Lin, J. Yang, Y. Nuli, Energy Environ. Sci. 5 (2012) 6966–6972.
[23] H. Wang, Y. Yang, Y. Liang, J.T. Robinson, Y. Li, A. Jackson, Y. Cui, H. Dai, Nano Lett. 11 (2011) 2644–2647.
[24] G.Y. Zheng, Q.F. Zhang, J.J. Cha, Y. Yang, W.Y. Li, Z.W. Seh, Y. Cui, Nano Lett. 13 (2013) 1265–1270.
[25] S. Xin, Y.X. Yin, L.J. Wan, Y.G. Guo, Part. Part. Syst. Char. 30 (2013) 321–325.
[26] L.X. Miao, W.K. Wang, A.B. Wang, K.G. Yuan, Y.S. Yang, J. Mater. Chem. A 1 (2013) 11659–11664.
[27] J.Q. Huang, Q. Zhang, H.J. Peng, X.Y. Liu, W.Z. Qian, F. Wei, Energy Environ. Sci. 7 (2014) 347–353.
[28] S.S. Zhang, Electrochim. Acta 70 (2012) 344–348.
[29] J. Song, T. Xu, M.L. Gordin, P. Zhu, D. Lv, Y.-B. Jiang, Y. Chen, Y. Duan, D. Wang, Adv. Funct. Mater. 24 (2014) 1243–1250.
[30] Q. Zhang, J.Q. Huang, M.Q. Zhao, W.Z. Qian, F. Wei, ChemSusChem 4 (2011) 864–889.
[31] Q. Zhang, J.-Q. Huang, W.Z. Qian, Y.-Y. Zhang, F. Wei, Small 9 (2013) 1237–1265.
[32] X.B. Cheng, J.-Q. Huang, Q. Zhang, H.J. Peng, M.-Q. Zhao, F. Wei, Nano Energy 4 (2014) 65–72.
[33] Q. Zhang, M.Q. Zhao, J.Q. Huang, Y. Liu, Y. Wang, W.Z. Qian, F. Wei, Carbon 47 (2009) 2600–2610.
[34] H.J. Peng, J.Q. Huang, M.Q. Zhao, Q. Zhang, X.B. Cheng, X.Y. Liu, W.Z. Qian, F. Wei, Adv. Funct. Mater. 24 (2014), http://dx.doi.org/10.1002/adfm.201303296.
[35] S.S. Zhang, K. Xu, T.R. Jow, Electrochim. Acta 49 (2004) 1057–1061.
[36] K. Jin, X. Zhou, L. Zhang, X. Xin, G. Wang, Z. Liu, J. Phys. Chem. C 117 (2013) 21112–21119.
[37] W. Zhou, H. Chen, Y. Yu, D. Wang, Z. Cui, F.J. DiSalvo, H.D. Abruña, ACS Nano 7 (2013) 8801–8808.
[38] T. Xu, J. Song, M.L. Gordin, H. Sohn, Z. Yu, S. Chen, D. Wang, ACS Appl. Mater. Interfaces 5 (2013) 11355–11362.
[39] J.Q. Huang, Q. Zhang, S.M. Zhang, X.F. Liu, W.C. Zhu, W.Z. Qian, F. Wei, Carbon 58 (2013) 99–106.
[40] S.H. Chung, A. Manthiram, Electrochim. Acta 107 (2013) 569–576.
[41] K. Zhang, F. Qin, J. Fang, Q. Li, M. Jia, Y. Lai, Z. Zhang, J. Li, J. Solid State Electr. 18 (2014) 1025–1029.
[42] H.S. Ryu, H.J. Ahn, K.W. Kim, J.H. Ahn, J.Y. Lee, E.J. Cairns, J. Power Sources 140 (2005) 365–369.
[43] S.S. Zhang, D.T. Tran, J. Power Sources 211 (2012) 169–172.
[44] S.-H. Chung, A. Manthiram, Electrochem. Commun. 38 (2014) 91–95.
[45] Y. Zhang, Z. Bakenov, Y. Zhao, A. Konarov, Q. Wang, P. Chen, Ionics (2014), http://dx.doi.org/10.1007/s11581-013-1042-7.
[46] S.H. Chung, A. Manthiram, J. Mater. Chem. A 1 (2013) 9590–9596.
[47] L. Wang, X.M. He, J.J. Li, J. Gao, M. Fang, G.Y. Tian, J.L. Wang, S.S. Fan, J. Power Sources 239 (2013) 623–627.
[48] H. Kim, J.T. Lee, G. Yushin, J. Power Sources 226 (2013) 256–265.
[49] X.F. Liu, Q. Zhang, J.Q. Huang, S.M. Zhang, H.J. Peng, F. Wei, J. Energy Chem. 22 (2013) 341–346.